Improved retrieval of cloud base heights from ceilometer using a non-standard instrument method

Yang Wang[a], Chuanfeng Zhao[a,b,*], Zipeng Dong[a,c], Zhanqing Li[a], Shuzhen Hu[d], Tianmeng Chen[a], Fa Tao[d], Yuzhao Wang[e]

[a] State Key Laboratory of Earth Surface Processes and Resource Ecology, and College of Global Change and Earth System Science, Beijing Normal University, Beijing 100875, China
[b] Division of Geological and Planetary Sciences, California Institute of Technology, Pasadena, CA 91125, USA
[c] Meteorological Institute of Shaanxi Province, Xi'an 710014, China
[d] Meteorological Observation Center, Chinese Meteorological Administration, Beijing 100081, China
[e] Laser Engineer Technology Laboratory, Beijing Institute of Space Mechanics and Electricity, Beijing 100094, China

ARTICLE INFO

ABSTRACT

Cloud-base height (CBH) is a basic cloud parameter but has not been measured accurately, especially under polluted conditions due to the interference of aerosol. Taking advantage of a comprehensive field experiment in northern China in which a variety of advanced cloud probing instruments were operated, different methods of detecting CBH are assessed. The Micro-Pulse Lidar (MPL) and the Vaisala ceilometer (CL51) provided two types of backscattered profiles. The latter has been employed widely as a standard means of measuring CBH using the manufacturer's operational algorithm to generate standard CBH products (CL51 MAN) whose quality is rigorously assessed here, in comparison with a research algorithm that we developed named value distribution equalization (VDE) algorithm. It was applied to both the profiles of lidar backscattering data from the two instruments. The VDE algorithm is found to produce more accurate estimates of CBH for both instruments and can cope with heavy aerosol loading conditions well. By contrast, CL51 MAN overestimates CBH by 400 m and misses many low level clouds under such conditions. These findings are important given that CL51 has been adopted operationally by many meteorological stations in China.

1. Introduction

Cloud base height (CBH) is one of the fundamental cloud variables (Hirsch et al., 2011) governing the surface radiation budget especially downward longwave radiation (Viúdez-Mora et al., 2015). It is a prerequisite to retrieve other cloud micro-physical properties (Martucci and O'Dowd, 2011; Garrett and Zhao, 2013). Many previous studies attempted to retrieve CBH from different satellite sensors (Forsythe et al., 2000; Hutchison, 2002; Hutchison et al., 2006; Meerkötter and Zinner, 2007; Sharma et al., 2016; Sun et al., 2016). All passive sensors aboard satellite are, however, inherently difficult to do so because the outgoing infrared radiance is much more sensitive to the IR emission from top of a cloud than its bottom (Kim et al., 2011), except for high-resolution sensors like VIIRS that may see cloud bases through their gaps (Zhu et al., 2014). Besides, the satellite CBH products often provide very few diurnal samples for any particular location (Martucci et al., 2010).

Ground-based active sensors can detect CBH much more readily and accurately (Goodman and Henderson-Sellers, 1988), at a high temporal resolution of much spatial coverage. Lidar and radar are two most useful sensors for observing cloud boundaries with complimentary merits due to their different spectral bands (Wang and Sassen, 2001; Garrett and Zhao, 2013). They have been employed to generate CBH climatology at the ARM South Great Plain (e.g. Dong et al., 2010; Xi et al., 2010) that can be used for evaluating cloud simulations by weather forecast model (e.g. Willén et al., 2005; Illingworth et al., 2012; Morcrette et al., 2012).

Lidar and cloud ceilometer have been much more widely employed than cloud radar for the determination of cloud bases and cloud occurrences (e.g., Clothiaux et al., 2000; Martucci et al., 2007; Zhao et al., 2012; Costa-Surós et al., 2013; Lee et al., 2017). Ceilometer, a low-energy lidar, has been used as an operational sensor at meteorological stations for providing continuous CBH data as a standard output product at a low cost during both day and night (Martucci et al., 2010;

Román et al., 2017). Its backscattering information may also be used to infer aerosol layer structures and atmospheric boundary layer heights (e.g., Zéphoris et al., 2005; Martucci et al., 2007; Morille et al., 2007; Schween et al., 2014).

While the gross feature of CBH can be readily obtained by any active sensor, it is still a challenge to acquire precise estimation of CBH (Clothiaux et al., 2000). To detect clouds from lidar measurements, algorithms have to distinguish signal changes from aerosol, clouds, and random noise, especially under heavy polluted conditions like China and India (Li et al., 2016). Without heavy aerosol loading, clear cloudy scenes can be differentiated by setting thresholds of the backscatter signals (Pal et al., 1992; Clothiaux et al., 2000), except for very thin clouds in a hazy boundary layer which requires a more delicate algorithm to detect the CBH.

Given the wide usage of ceilometers in CBH detection, the accuracy of derived CBHs is thoroughly evaluated in this study and a more accurate method than the conventional one is developed in this study. The manufacturer operational CBH products from Vaisala ceilometer (CL51 MAN) is evaluated against other CBH products generated from a micropulse lidar (MPL) and from a ceilometer by Vaisala CL51 using our Value Distribution Equalization (VDE) algorithm (Zhao et al., 2014), along with the CBHs determined from radiosonde profiles of atmospheric humidity.

Section 2 describes the field experiments, instruments, datasets and methods used in the study. Analyses of the MPL and CL51 CBH products and improvement are elaborated in Section 3. Section 4 summarizes the study.

2. Data and methods

2.1. Field campaign

A field experiment named the Atmosphere-Aerosol-Boundary Layer-Cloud (A^{2}BC) Interaction Joint Experiment was carried out at the Xingtai meterological station (37.18°N, 114.37°E, 183 m above the mean sea level) from May 1 to December 31 in 2016, with an intensive observation period (IOP) from May 1 to June 15 in 2016. Only the measurements made during the IOP were examined in this study. The site of the experiment was at the eastern foot of Taihang Mountain, 18.5 km away from the small city of Xingtai and 96.1 km away from the big city of Shijiazhuang, where air pollution is among the worst in China. Fig. 1 is a map showing the city locations (marked as red dots) and the topography distribution around the field campaign site (marked as yellow dot).

2.2. Instruments

The data we used in this study are from the following instruments: (1) The Millimeter-wavelength Cloud Radar (MMCR), (2) the MPL, (3) the Vaisala CL51, (4) the Total Sky Imager (TSI), and (5) the Radiosonde. Table 1 shows the information about these instruments, which will also be described in detail below. Note that all these ground-based instruments were placed no more than 30 m from each other.

2.2.1. Micro pulse lidar (MPL)

The MPL is a ground-based lidar which can be used to determine the altitude of clouds overhead, with an eye-safe pulse energy at a wavelength of 532 nm from the Nd: YLF. In addition to the real-time detection of clouds, the subsequent processing of the lidar signal returns can also broaden their advantages to characterize the properties of aerosols, boundary layer structure as well as the evolution of pollutants in heavily particle-laden regions (Satheesh et al., 2006; Zhao et al., 2014). The MPL instrument used in this study is manufactured by Sigma Space Corporation (Spinhirne, 1993; Mendoza and Flynn, 2006). It transmits laser pulses into the atmosphere and subsequently measures the intensity of backscattered light using photon-counting detectors and
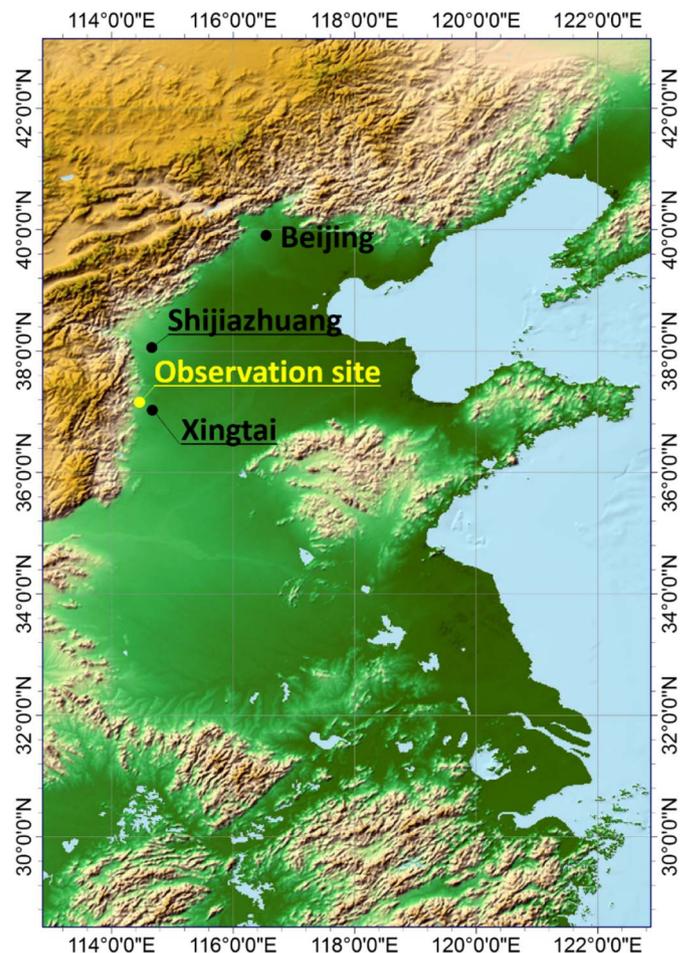
Fig. 1. The location of the field campaign (marked by yellow point) and the topography surrounded the observation site. Also marked are the three cities of Beijing, Shijiazhuang, and Xingtai in this region. (For interpretation of the references to color in this figure legend, the reader is referred to the web version of this article.)

Table 1
Characteristics of the instruments used in this study during our field campaign at Xingtai site.

Instrument	Temporal/spatial resolution	Wavelength/ frequency	Observed or derived quantity
MPL	30 s/30 m	532 nm	Altitude of clouds
MMCR	60 s/15 m	35 GHz	Reflectivity factor, Doppler velocity, Doppler width
CL51	36 s/10 m	910 nm	Altitude of clouds
TSI	10 min/–	–	Cloud fraction
Radiosonde	1 s/–	–	Profiles of relative humidity, pressure and temperature

The mark "–" represents no value in the table.

transforms the signal into atmospheric information. In this study, the backscattered light is processed as normalized relative backscatter (NRB) (Campbell et al., 2002) and is then adopted by our VDE algorithm for CBH detection (MPL VDE). The MPL observation time resolution is 30 s and the vertical spatial resolution is set as 30 m with a maximum detection altitude of 20 km.

2.2.2. Vaisala CL51

As a single-wavelength backscatter lidar, Vaisala CL51 is a laser ceilometer with the ability to determine the altitude of clouds automatically and continuously with the near infrared 910 nm to avoid

strong Rayleigh scattering. The pulse energy of CL51 is low enough to allow eye-safe operation. The temporal resolution we used in our field campaign is 36 s and the vertical spatial resolution is about 15 m with a maximum detection height of 15 km. In addition to the CBH datasets obtained directly from the manufactory operational outputs called CL51 MAN, we also make full use of the backscatter profiles in CL51 to derive the CBH from our VDE algorithm (CL51 VDE).

2.2.3. Millimeter-wavelength radar (MMCR)

The MMCR used in this study is developed by the Xi'an Huateng Microwave cooperation, which is a fully coherent radar operating at a frequency of 35 GHz (Ka-band). It has a 30 m vertical resolution and 1 minute time resolution. The minimum detectable radar reflectivity can reach − 40 dBZ and the maximum detectable height is up to 20 km. The cloud radar is sensitive to small hydrometeors owing to its short wavelength relative to the conventional weather or precipitation radars (Kollias et al., 2007). It is equipped with dual polarization, and thus can provide information about the phase of particles in clouds. Its range gate number is 500, but usually the measurements for the first eighteen gates are invalid (Kollias et al., 2007). Different pulse width options are available to detect different kinds of clouds (Zhong et al., 2011). A narrow pulse width mode is suitable for observing low clouds, while a long pulse width mode provides high sensitivity and can detect optically thin clouds, such as cirrus. All of these factors make this radar an ideal tool for cloud detection, especially for low and middle clouds, which are tough to penetrate for MPL and CL51.

2.2.4. Radiosonde

Radiosonde can obtain detailed vertical profiles of temperature, relative humidity, pressure, horizontal wind speed, and wind direction in the time resolution of one second. Typically, the sounding balloons are released twice a day at fixed time 07:15 and 19:15 Beijing Time (BJT) over Xingtai weather station. During the IOP field campaign, the third radiosonde balloon is required to be launched at about 13:00 BJT every day.

In this study, the CBHs retrieved from the radiosonde are used as another method to verify the performance of MPL and CL51. For the CBHs reported by the radiosonde, we use the algorithm proposed by Zhang et al. (2010) which identifies cloud bases according to relative humidity (RH) using the following criteria: The location of cloud base is determined when the minimum RH of the layer is above 84% and there are more than 3% jumps in RH during the transition from the sky below the layer to the base of the cloud layer. If the maximum RH is above 87%, the layer is considered to be a cloud. Note that the RH represents the relative humidity with respect to ice when the temperature is below 0 °C.

2.2.5. Total sky imager

The total sky imager (TSI) uses an installed digital camera, looking downwards toward a rotating hemispheric mirror, to automatically record the sky condition. The digital images are then stored into compressed format in images which convey information on the relative red, green, and blue element that goes into making up a real pixel's color (Long et al., 2006). We often use the red to blue pixel ratio values to distinguish whether a pixel represents a clear or cloudy portion of the sky image and to estimate the fraction of opaque/thin clouds in the image of the total sky (Long et al., 2001). In this study, the TSI images are stored in the order of 10 min during the day time from sunrise to sunset.

2.3. Methods

In this study, we apply our VDE algorithm to both the CL51 and MPL backscatter laser signal to obtain the CBH products of CL51 VDE and MPL VDE, respectively. The VDE algorithm can somehow inhibit the impact of increasing noise with distance due to range correction and

thus reduce the magnitude of signal variations with distance (Zhao et al., 2014). The VDE algorithm can separate clouds and aerosols with high accuracy, and is suitable for heavy polluted conditions over our campaign site at Xingtai, Heibei province. More details about the VDE algorithm are described in Zhao et al. (2014).

We should note that cloud base height from both CL51 and MPL are the heights estimated based on the vertical information, ignoring the spatial dimensions and excluding some clouds which are not in the vertical line of CL51 and MPL (Román et al., 2017). Actually, the cloud base heights determined from radiosonde profiles of temperature and relative humidity are also based on the vertical information, but the balloon could move with air at horizontal direction. Thus, in order to make CBHs detected by radiosonde to be compared with the CBHs derived from MPL and CL51, we only use the cases in section 3 that 1) the cloud base height variation is small and the sky is overcast, and 2) the boundary layer clouds which both the radiosonde and MPL can detect the same since the radiosonde can reach the cloud layer in just minutes near the place set free. Even so, the differences in vertical locations introduced by the horizontal movement from radiosonde still exist and are not considered in this study.

3. Results and discussions

An objective of our study is to check if the VDE algorithm is valid for the CL51, for it was developed for use with a MPL, and another objective is to cross compare them in terms of discrepancies resulting from different instruments and different algorithms. To this end, we have generated CBH products from radiosonde, MPL using the VDE algorithm, and two products from ceilometer using both the manufacture algorithm and the VDE method, as well as from the MMCR, with reference to TSI images.

3.1. The performance of CBHs from MPL using VDE algorithm

The advantages of MPL VDE in cloud detection have been described in Zhao et al. (2014). In this study, we evaluate the reliability of MPL VDE in the determination of CBHs under polluted cases. Fig. 2 shows a case in May 21, 2016 when the day is heavily polluted (with the daily averaged aerosol number concentration of 12,881 cm^{-3} from the ground observation) within the boundary layer of height ∼1900 m, which can also be demonstrated by the aircraft measurements conducted from 13:00 to 15:00 BJT. The flight observations show that aerosols are well mixed and the aerosol number concentration is high within the boundary layer but the number concentration decreases dramatically at the top of boundary layer which is about 1900 m.

Fig. 2 a, b and c show the MMCR radar reflectivity, CL51 back scattering signal, MPL back scattering signal, respectively. As known, the MMCR radar has much stronger penetration capability than MPL and Ceilometer, which can detect high level clouds as shown at time roughly between 17:00 and 23:00 BJT and cloud tops. On the other hand, the CBHs detected by MMCR often have large uncertainties and MMCR often misses thin cloud layers, such as those thin clouds at heights around 5 km occurred between 18:00 and 24:00 BJT. Thus, MPL and CL51 have their advantages in detecting low level clouds and identifying accurate cloud bases, including those thin clouds, while they could miss top layers of multi-layer clouds. Fig. 2 d, e and f illustrate the clouds detected by CL51 MAN, CL51 VDE and MPL VDE, respectively. They have demonstrated their ability to detect the thin cloud layers at heights around 5 km from 18:00 and 24:00 BJT. From 12:00 to 16:00 BJT, the sky is dotted with small shallow convective clouds as shown in Fig. 3, which are also detected by MPL and CL51 as denoted by the black points in Fig. 2 d, e, and f.

Both the CL51 MAN and CL51 VDE fail to identify the boundary clouds detected by MPL VDE after 19:00 BJT on that day. To examine if the boundary layer clouds exist, the radiosonde profile launched at 19:15 BJT has been examined. As shown in Fig. 4, the radiosonde
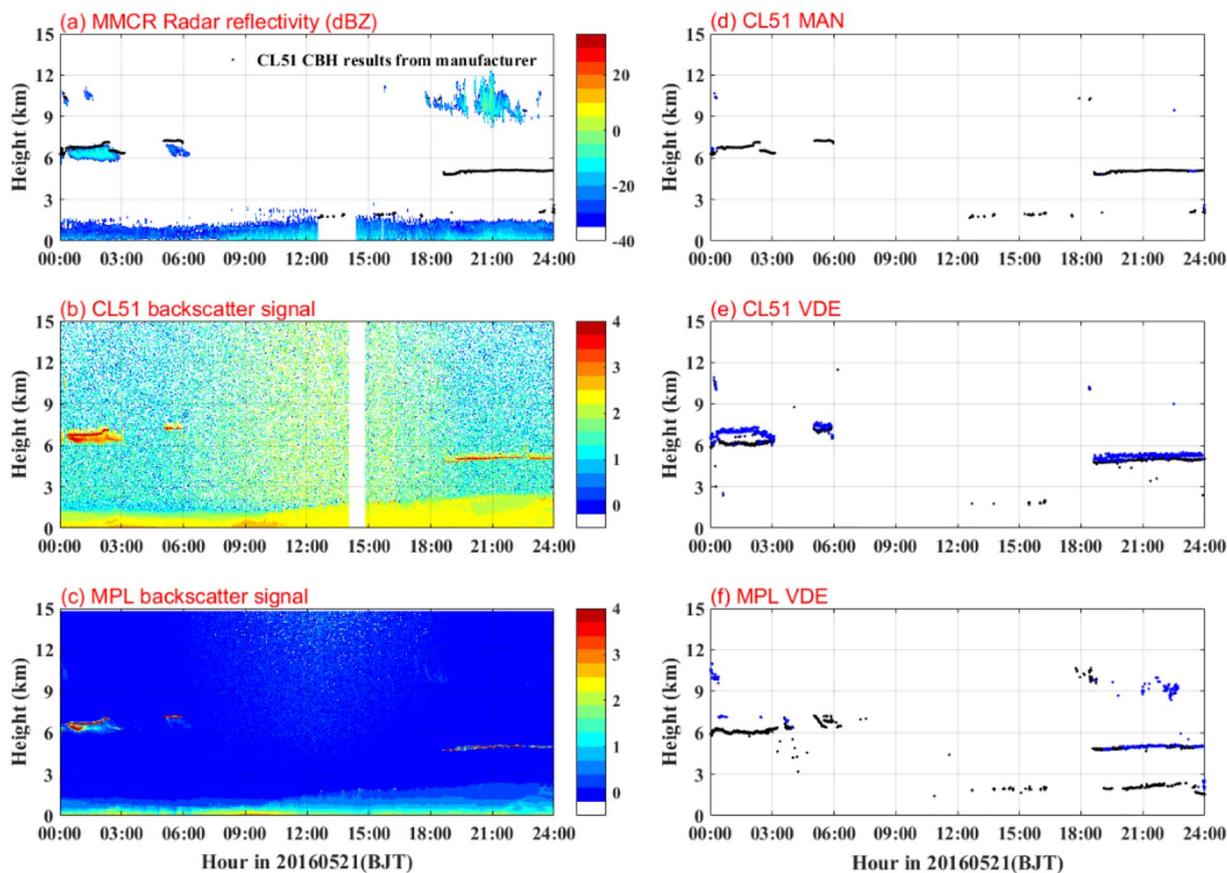
Fig. 2. The time–height cross section of (a) MMCR radar reflectivity overlaid CL51 CBHs from manufacturer (the first and second cloud layers are dotted in black color), (b) CL51 backscatter signal, (c) MPL backscatter signal, (d) CL51 CBHs from manufactory operational products, (e) CL51 CBHs from VDE algorithm, and (f) MPL CBHs from VDE algorithm, at Xingtai site on May 21, 2016. For the Figures (d), (e), and (f), the black dots represent the first CBHs and the blue ones are the second CBHs. (For interpretation of the references to color in this figure legend, the reader is referred to the web version of this article.)

profile clearly shows the existence of that boundary cloud layer. It detects this boundary cloud layer and a second cloud layer with the CBHs of 1893 m and 4842 m, respectively. By contrast, the CBHs derived from the MPL VDE are 1919 m (the first cloud layer) and 4826 m (the second cloud layer) averaged in 3 min centered around the time when the radiosonde detects cloud layers. The similar CBHs detected by MPL VDE and radiosonde indicate that MPL VDE can detect both the first and second cloud layers reliably. By contrast, the CL51 failed to identify the first boundary layer clouds even with the VDE algorithm. The relatively worse performance of CL51 compared to MPL is most likely associated with its much lower pulse energy and much smaller signal to noise ratios (SNRs), which makes it more difficult to identify the boundary layer clouds that are often contaminated by aerosols, particularly for thin clouds. In addition to the low level boundary clouds, the MPL VDE has superior performance in high level cloud detection as indicated by Zhao et al. (2014). This can be illustrated by
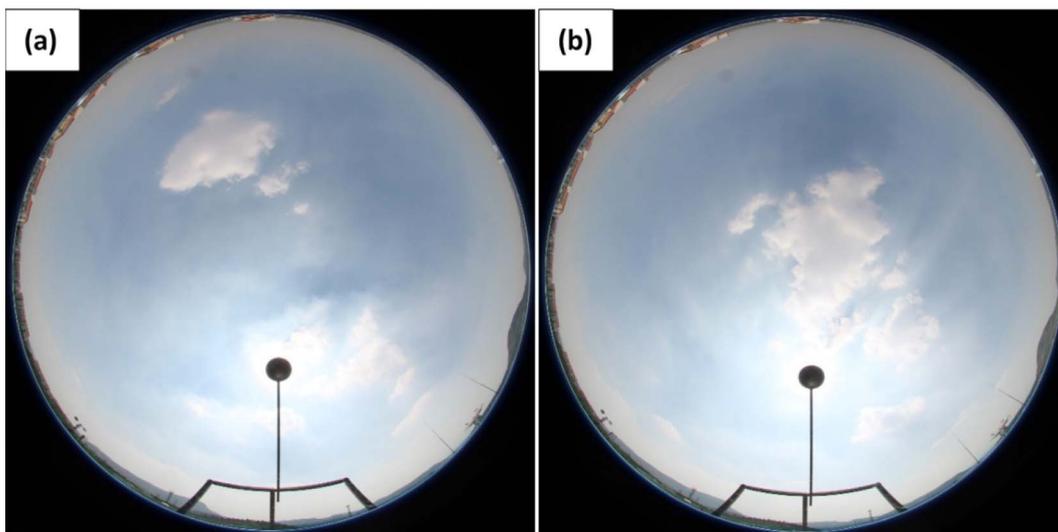
Fig. 3. The TSI images taken at 14:20 (a) and 14:30 (b) BJT on May 21, 2016.
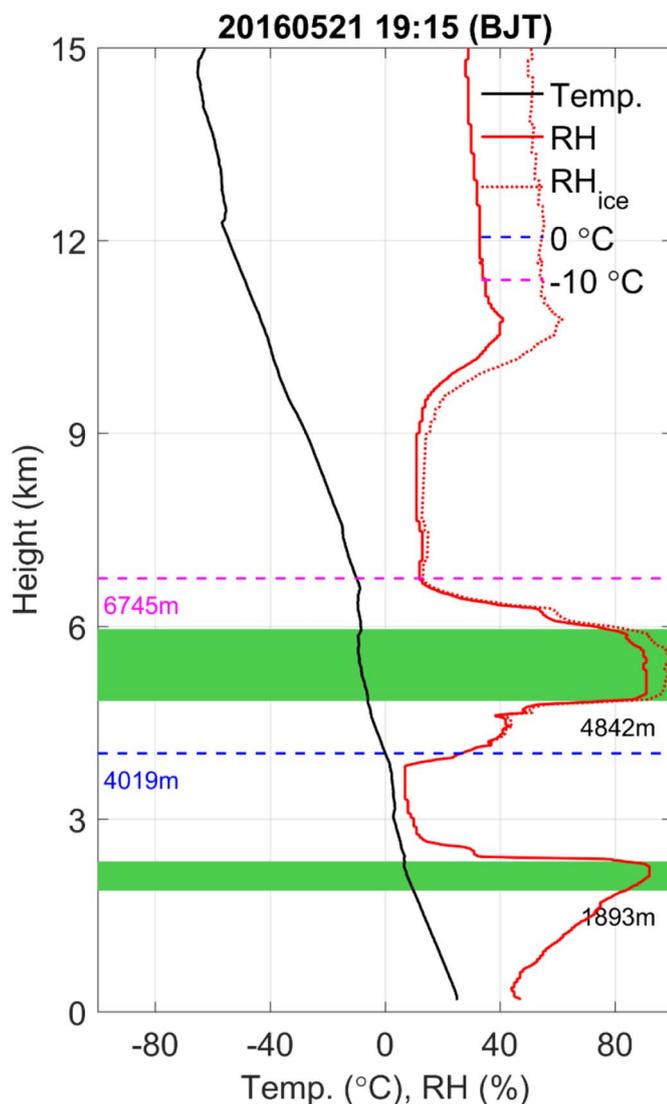
Fig. 4. The profiles of the temperature, relative humidity, and relative humidity with respect to ice. The blue and purple dashed lines show the temperature of 0 °C and − 10 °C, respectively, with the corresponding color text denoting the height for each specific temperatures. The green areas indicate the cloud layers detected by the radiosonde with black texts below showing the cloud base heights of each cloud layers. (For interpretation of the references to color in this figure legend, the reader is referred to the web version of this article.)

Fig. 2f, in which MPL VDE detects high clouds around 4826 m and partial of those high clouds above 9 km.

Considering the reliability of CBHs obtained from the MPL VDE, they will be used in the evaluation of CL51 MAN and the VDE algorithm will be adopted to reprocess the signals from CL51 to get a better CBHs product CL51 VDE, which will be shown in section 3.2.

3.2. The improvement of CBHs from CL51 using VDE algorithm

Lee et al. (2017) have shown the better performance of CL51 than CL31, which is another type of Ceilometer, and found that CL51 can retrieve cloud base heights and backscatter profiles up to 13 and 15 km. They showed the climatology of CBHs over Seoul using CL51 MAN, and indicated that the limitation of CL51 in detecting upper layer clouds, which could miss about 10–25%. We here examine the performance of CBHs detection from CL51 by using VDE algorithm.

As the case shown in Fig. 2, the cloud base heights derived from the CL51 MAN between 0:00 and 3:00 BJT are higher than the results from CL51 VDE on May 21, 2016. Actually, the CBHs from CL51 VDE are

roughly the same as those from MPL VDE with values about 6 km, but CBHs from CL51 MAN are close to the cloud tops. For the very thin clouds at night after 18:00 BJT on that day, CBHs from the three products are in good consistency. Similar results that CBHs from CL51 MAN are overestimated except for thin clouds have been found for other cases during the one-month observation period. It suggests that the CBHs retrieved from CL51 VDE might be more reliable (agree well with MPL VDE product) compared to the CL51 MAN product.

The overestimation of CBHs from CL51 MAN compared to those from CL51 VDE is mainly caused by their different applied retrieval algorithms. The CBH in CL51 MAN product defines the cloud base as the height at which the backscattered signal reaches its maximum value in each profile (Eberhard, 1986), which leads to the location of CBH somewhat inside the cloud (overestimated CBHs). The VDE algorithm, however, could discriminate the typically sharp signal change at the altitude just around the cloud base with its advantage to reject the discriminations of small changes caused by the signal noises or aerosol returns.

This advantage of VDE algorithm can be further verified in Fig. 5, which shows another case on June 1, 2016 when there is a thin low level cloud covered in the sky. As expected, both CL51 and MPL have relatively weaker penetration capability and cannot detect the top parts of the high clouds found at heights around 6–11 km as demonstrated by MMCR in Fig. 5a. However, they can detect the low thin clouds at heights around 1.8 km as shown in Figs. 5 b and c, which have not been captured by the MMCR in Fig. 5 a. Both the MPL VDE and CL51 VDE can clearly detect the low level clouds most of the time with cloud base height of about 1700 m on average, which are shown in Figs. 5 e and f. Fig. 6 further shows the radiosonde profiles of temperature and relative humidity launched at 7:16 BJT and 19:19 BJT on June 1, 2016. The low level CBHs derived from the radiosonde launched at 7:16 BJT are 1704 m and 1997 m, and the CBH is 1712 m at 19:19 BJT. It shows great consistency between the results retrieved from MPL VDE and CL51 VDE and the results from radiosonde. But the CL51 MAN misses these low level cloud layers most of the day as shown in Fig. 5d, which is most likely due to the challenge of classification between aerosol and clouds by CL51 MAN. Similarly, we can also see clearly that CL51 MAN overestimates the CBHs of thick clouds at heights around 6 km after 21:00 BJT compared with MPL VDE and CL51 VDE.

Since MPL VDE and the CL51 VDE apply the same algorithm, the discrepancies between them are primarily caused by the differences between the two instruments including the wavelength (532 nm vs 910 nm), pulse energy, system parameter and so on. All of these lead to the different signal to noise ratios (SNRs) between them. In general, the SNR of MPL is much higher than the CL51 mainly due to higher pulse energy of MPL. When the SNR is too low, especially at time around the noon when the solar radiation is the strongest, the VDE algorithm may also miss the detection of cloud layer, as shown by CL51 VDE in Fig. 5e around 12:00 BJT.

In short summary, the CBHs from CL51 VDE is much more reliable than those from the CL51 MAN considering the overestimation of CBHs for thick clouds and the likely misidentification of boundary layer clouds in CL51 MAN product.

3.3. Statistical evaluation of CBHs from CL51 MAN and CL51 VDE

Though the MPL performs more reliably than the CL51 does in the detection of clouds, the CL51 is less expensive and needs much less manual operation to maintain its running, which makes it a cost-effective instrument to be widely employed (An et al., 2017). Thus, it is important to know to what extent the VDE algorithm applied to CL51 will improve the performance of CBHs compared with the manufactory outputs. Here we quantify this using statistical analysis by conducting the comparisons between CL51 VDE and MPL VDE, and between the CL51 VDE and CL51 MAN. Since the CBHs in the products of all the instruments are most accurate for the lowest clouds, we only do the
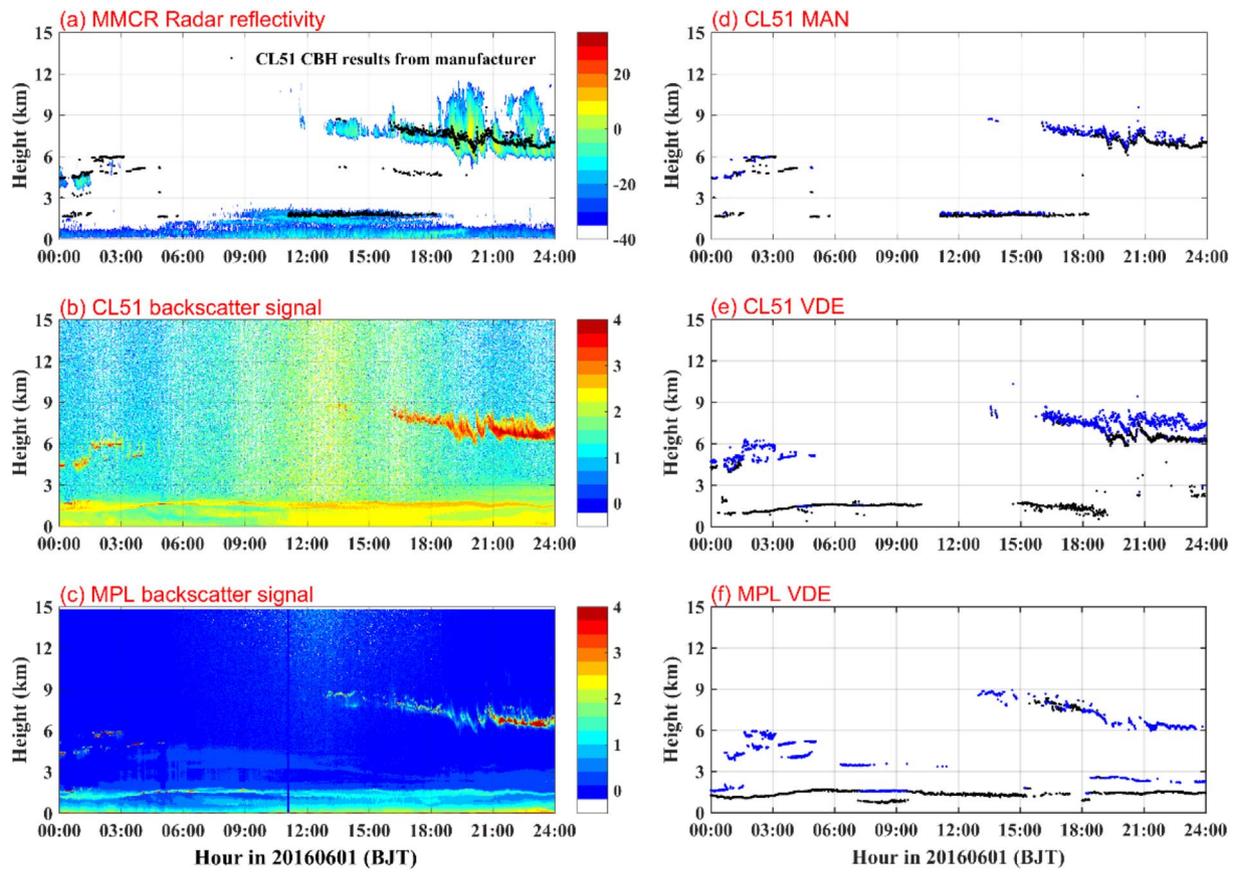
Fig. 5. The same as Fig. 2, but on June 1, 2016.
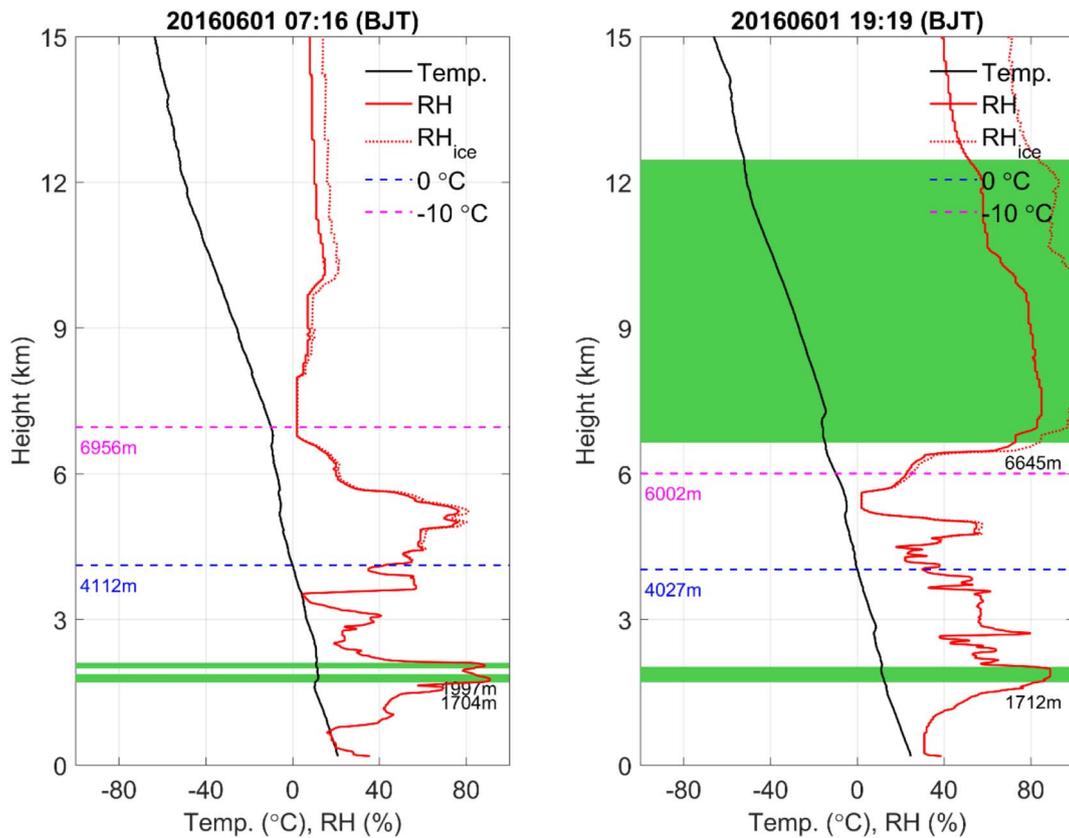
Fig. 6. The same as Fig. 4, but on June 1, 2016.
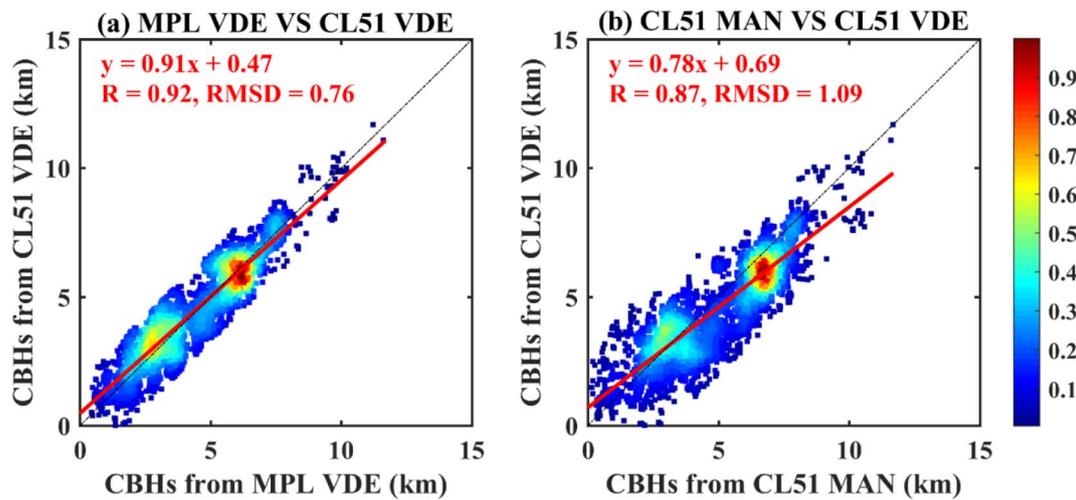
Fig. 7. The scatterplots of the first cloud base height observed in our field campaign (a) between using MPL VDE and using CL51 VDE, and (b) between using CL51 VDE and using CL51 MAN. For each panel, the red line and black dashed line represent the fitting regression line and the 1:1 line, respectively. The liner equation, correlation coefficient (R), and root mean square deviation (RMSD) are shown in red text. The color bar shows the data (scatter points) density with the densest (equal to 1) in red color and the sparsest (equal to 0) in blue color. (For interpretation of the references to color in this figure legend, the reader is referred to the web version of this article.)

comparisons using the first layer cloud base heights in each product during the IOP in our field campaign.

Fig. 7 shows the statistical inter-comparison results of CBHs between MPL VDE and CL51 VDE, and between CL51 MAN and CL51 VDE. The data are used only when the CBHs in all the three products are simultaneously valid. It shows that the correlation coefficient and root mean square difference (RMSD) between the CL51 VDE and MPL VDE are much better, with values of 0.92 and 0.76 km, respectively. With the knowledge that MPL VDE performs more credibly as shown earlier, the results in Fig. 7 suggest the good performance of the VDE algorithm when applied to the CL51 backscatter profiles. In contrast, the correlation coefficient and RMSD between the CL51 MAN and CL51 VDE are 0.87 and 1.09 km, respectively. The linear fitting regression line indicates the overestimated CBHs in CL51 MAN compared with CL51 VDE.

Fig. 8 further shows the statistical results in each product in our field campaign during this month. The mean CBH value in CL51 MAN is

4974.6 m while the CL51 VDE and MPL VDE CBHs are very close to each other with the values of 4570.7 m and 4520.3 m, respectively. The much smaller differences in CBHs between CL51 and MPL when applying the VDE algorithm, suggest that the CBH differences associated with the retrieval algorithms (VDE vs MAN) could be much larger than that associated with the instruments (CL51 vs MPL). On average, it shows that CBH form CL51 MAN is about 404 m higher than that from CL51 VDE in the study period and is overestimated about 454 m with respect to MPL VDE product. Actually, this overestimation can significantly affect the radiation budget analysis. As indicated by Viúdez-Mora et al. (2015), an error of 100 m in CBH may produce an error of up to 1.5 W/m^2 in the cloud radiative effect at the surface.

4. Summary

MPL can obtain the best estimate of CBHs when using the value distribution equalization algorithm (MPL VDE), even for very high and
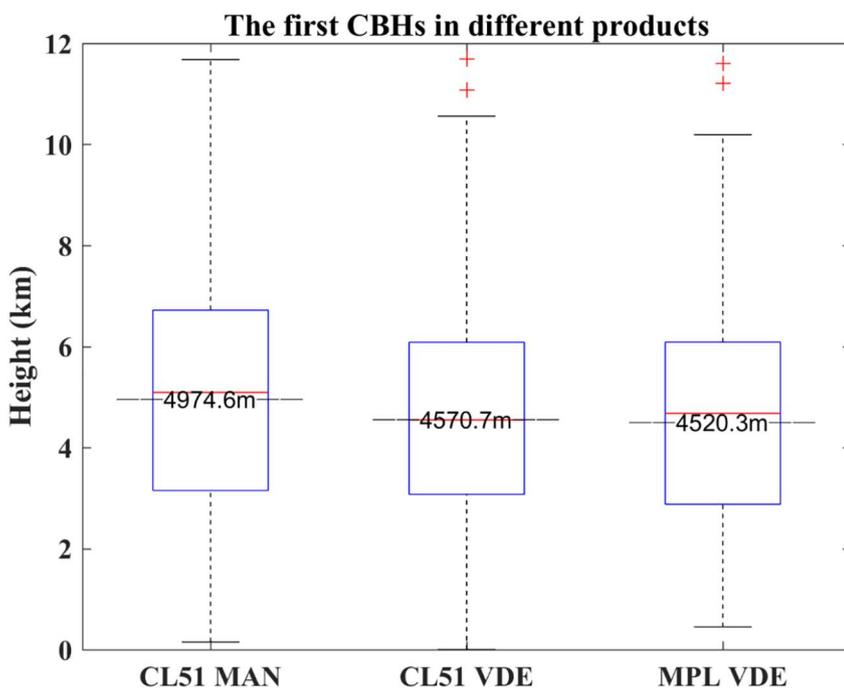
Fig. 8. The boxplots of the cloud base height of the first cloud layer observed in our field campaign in all the three products, i.e. CL51 from the manufactory outputs (CL51 MAN), the CL51 retrieved from VDE algorithm (CL51 VDE), and the MPL retrieved from VDE algorithm (MPL VDE). The black texts and black lines show the mean values in each products.

thin cloud layers or for low level clouds with aerosol noises. This has been illustrated based on radiosonde profile measurements of relative humidity and TSI images. The performance of CL51 in the determination of CBHs is much improved when we apply the value distribution equalization algorithm to the CL51 backscatter profiles (CL51 VDE). The CBH performance of CL51 VDE compared to CL51 manufactory operational outputs (CL51 MAN) has been evaluated with the MPL VDE product.

Compared to the manufactory outputs, the CBHs in CL51 VDE show better agreements with those in MPL VDE. On average, for the examined IOP field campaign, the CL51 MAN overestimates the CBHs about 404 m compared to the CL51 VDE. In addition, the CL51 VDE can detect more low level clouds reliably under the aerosol polluted conditions, which is very important in Eastern China where the air pollution is often severe. Our study suggests that there are considerable overestimated biases in the manufactory product of CL51 and the CBHs from CL51 could be highly improved by applying the value distribution equalization algorithm. This finding is particularly important considering that CL51 is being adopted operationally by many meteorological stations in China.

Acknowledgements

References

An, N., Wang, K., Zhou, C., Pinker, R.T., 2017. Observed variability of cloud frequency and cloud-base height within 3600 m above the surface over the contiguous United States. J. Clim. 30, 3725–3742.

Campbell, J.R., Hlavka, D.L., Welton, E.J., Flynn, C.J., Turner, D.D., Spinhirne, J.D., Scott III, V.S., Hwang, I., 2002. Full-time, eye-safe cloud and aerosol lidar observation at atmospheric radiation measurement program sites: instruments and data processing. J. Atmos. Ocean. Technol. 19, 431–442.

Clothiaux, E.E., Ackerman, T.P., Mace, G.G., Moran, K.P., Marchand, R.T., Miller, M.A., Martner, B.E., 2000. Objective determination of cloud heights and radar reflectivities using a combination of active remote sensors at the ARM CART sites. J. Appl. Meteorol. 39, 645–665.

Costa-Surós, M., Calbó, J., González, J., Martin-Vide, J., 2013. Behavior of cloud base height from ceilometer measurements. Atmos. Res. 127, 64–76.

Dong, X., Xi, B., Crosby, K., Long, C.N., Stone, R.S., Shupe, M.D., 2010. A 10 year climatology of Arctic cloud fraction and radiative forcing at Barrow, Alaska. J. Geophys. Res.-Atmos. 115.

Eberhard, W.L., 1986. Cloud signals from lidar and rotating beam ceilometer compared with pilot ceiling. J. Atmos. Ocean. Techn. 4, 499–512.

Forsythe, J.M., Vonder Haar, T.H., Reinke, D.L., 2000. Cloud-base height estimates using a combination of meteorological satellite imagery and surface reports. J. Appl. Meteorol. 39, 2336–2347.

Garrett, T., Zhao, C., 2013. Ground-based remote sensing of thin clouds in the Arctic. Atmos. Meas. Tech. 6, 1227–1243.

Goodman, A.H., Henderson-Sellers, A., 1988. Cloud detection and analysis: a review of recent progress. Atmos. Res. 21 (3), 203–228.

Hirsch, E., Agassi, E., Koren, I., 2011. A novel technique for extracting clouds base height using ground based imaging. Atmos. Meas. Tech. 4, 117.

Hutchison, K., 2002. The retrieval of cloud base heights from MODIS and three-dimensional cloud fields from NASA's EOS aqua mission. Int. J. Remote Sens. 23, 5249–5265.

Hutchison, K., Wong, E., Ou, S., 2006. Cloud base heights retrieved during night-time conditions with MODIS data. Int. J. Remote Sens. 27, 2847–2862.

Illingworth, A.J., Hogan, R.J., O'Connor, E.J., et al., 2012. Continuous evaluation of cloud profiles in seven operational models using ground-based observations. Bull. Amer. Meteorol. Soc. 88 (6), 883–898.

Kim, S.-W., Chung, E.-S., Yoon, S.-C., Sohn, B.-J., Sugimoto, N., 2011. Intercomparisons of cloud-top and cloud-base heights from ground-based Lidar, CloudSat and CALIPSO measurements. Int. J. Remote Sens. 32, 1179–1197.

Kollias, P., Clothiaux, E., Miller, M., Albrecht, B., Stephens, G., Ackerman, T., 2007. Millimeter-wavelength radars: new frontier in atmospheric cloud and precipitation research. Bull. Amer. Meteorol. Soc. 88, 1608–1624.

Lee, S., Hwang, S.O., Kim, J., Ahn, M.H., 2017. Characteristics of cloud occurrence using ceilometer measurements and its relationship to precipitation over Seoul. Atmos. Res. 201, 46–57.

Li, Z., Lau, W.M., Ramanathan, V., et al., 2016. Aerosol and monsoon climate interactions over Asia. Rev. Geophys. 54, 866–929.

Long, C., Slater, D., Tooman, T., 2001. Total Sky Imager Model 880 Status and Testing Results. DOE Office of Science Atmospheric Radiation Measurement (ARM) Program (United States).

Long, C.N., Sabburg, J.M., Calbó, J., Pagès, D., 2006. Retrieving cloud characteristics from ground-based daytime color all-sky images. J. Atmos. Ocean. Technol. 23, 633–652.

Martucci, G., O'Dowd, C., 2011. Ground-based retrieval of continental and marine warm cloud microphysics. Atmos. Meas. Tech. 4, 2749–2765.

Martucci, G., Matthey, R., Mitev, V., Richner, H., 2007. Comparison between backscatter lidar and radiosonde measurements of the diurnal and nocturnal stratification in the lower troposphere. J. Atmos. Ocean. Technol. 24, 1231–1244.

Martucci, G., Milroy, C., O'Dowd, C.D., 2010. Detection of cloud-base height using Jenoptik CHM15K and Vaisala CL31 ceilometers. J. Atmos. Ocean. Technol. 27, 305–318.

Meerkötter, R., Zinner, T., 2007. Satellite remote sensing of cloud base height for convective cloud fields: a case study. Geophys. Res. Lett. 34.

Mendoza, A., Flynn, C., 2006. Micropulse Lidar (MPL) Handbook. The US Department of Energy.

Morcrette, C.J., O'Connor, E.J., Petch, J.C., 2012. Evaluation of two cloud parametrization schemes using ARM and cloud-net observations. Q.J.R. Meteorol. Soc. 138, 964–979.

Morille, Y., Haeffelin, M., Drobinski, P., Pelon, J., 2007. STRAT: an automated algorithm to retrieve the vertical structure of the atmosphere from single-channel lidar data. J. Atmos. Ocean. Technol. 24, 761–775.

Pal, S.R., Steinbrecht, W., Carswell, A.I., 1992. Automated method for lidar determination of cloud-base height and vertical extent. Appl. Opt. 31, 1488–1494.

Román, R., Cazorla, A., Toledano, C., Olmo, F.J., Cachorro, V.E., de Frutos, A., Alados-Arboledas, L., 2017. Cloud cover detection combining high dynamic range sky images and ceilometer measurements. Atmos. Res. 196, 224–236.

Satheesh, S., Vinoj, V., Moorthy, K.K., 2006. Vertical distribution of aerosols over an urban continental site in India inferred using a micro pulse lidar. Geophys. Res. Lett. 33.

Schween, J., Hirsikko, A., Löhnert, U., Crewell, S., 2014. Mixing-layer height retrieval with ceilometer and Doppler lidar: from case studies to long-term assessment. Atmos. Meas. Tech. 7, 3685–3704.

Sharma, S., Vaishnav, R., Shukla, M.V., Kumar, P., Kumar, P., Thapliyal, P.K., Lal, S., Acharya, Y.B., 2016. Evaluation of cloud base height measurements from ceilometer CL31 and MODIS satellite over Ahmedabad, India. Atmos. Meas. Tech. 9, 711–719.

Spinhirne, J.D., 1993. Micro pulse lidar. IEEE Trans. Geosci. Remote 31, 48–55.

Sun, X., Li, H., Barker, H., Zhang, R., Zhou, Y., Liu, L., 2016. Satellite-based estimation of cloud-base heights using constrained spectral radiance matching. Q. J. R. Meteorol. Soc. 142, 224–232.

Viúdez-Mora, A., Costa-Surós, M., Calbó, J., González, J., 2015. Modeling atmospheric longwave radiation at the surface during overcast skies: the role of cloud base height. J. Geophys. Res.-Atmos. 120, 199–214.

Wang, Z., Sassen, K., 2001. Cloud type and macrophysical property retrieval using multiple remote sensors. J. Appl. Meteorol. 40, 1665–1682.

Willén, U., Crewell, S., Baltink, H.K., Sievers, O., 2005. Assessing model predicted vertical cloud structure and cloud overlap with radar and lidar ceilometer observations for the Baltex bridge campaign of CLIWA-NET. Atmos. Res. 75 (3), 227–255.

Xi, B., Dong, X., Minni, P., Khaiyer, M.M., 2010. A 10 year climatology of cloud fraction and vertical distribution derived from both surface and GOES observations over the DOE ARM SPG site. J. Geophys. Res.-Atmos. 115.

Zéphoris, M., Holin, H., Lavie, F., Cenac, N., Cluzeau, M., Delas, O., ... Thibord, C., 2005. Ceilometer observations of aerosol layer structure above the petit Luberon during ESCOMPTE's IOP 2. Atmos. Res. 74 (1), 581–595.

Zhang, J., Chen, H., Li, Z., Fan, X., Peng, L., Yu, Y., Cribb, M., 2010. Analysis of cloud layer structure in Shouxian, China using RS92 radiosonde aided by 95 GHz cloud radar. J. Geophys. Res.-Atmos. 115.

Zhao, C., Xie, S., Klein, S.A., Protat, A., Shupe, M.D., McFarlane, S.A., Comstock, J.M., Delanoë, J., Deng, M., Dunn, M., 2012. Toward understanding of differences in current cloud retrievals of ARM ground-based measurements. J. Geophys. Res.-Atmos. 117.

Zhao, C., Wang, Y., Wang, Q., Li, Z., Wang, Z., Liu, D., 2014. A new cloud and aerosol layer detection method based on micropulse lidar measurements. J. Geophys. Res.-Atmos. 119, 6788–6802.

Zhong, L., Liu, L., Feng, S., Ge, R., Zhang, Z., 2011. A 35-GHz polarimetrie Doppler radar and its application for observing clouds associated with typhoon Nuri. Adv. Atmos. Sci. 28, 945.

Zhu, Y., Rosenfeld, D., Yu, X., Liu, G., Dai, J., Xu, X., 2014. Satellite retrieval of convective cloud base temperature based on the NPP/VIIRS imager. Geophys. Res. Lett. 41, 1308–1313.